Simulating the neutrino flux from the Spallation Neutron Source for the COHERENT experiment

D. Akimov,[1] P. An,[2,3] C. Awe,[2,3] P. S. Barbeau,[2,3] B. Becker,[4] V. Belov,[5,1] I. Bernardi,[4] M. A. Blackston,[6] C. Bock,[7] A. Bolozdynya,[1] J. Browning,[8] B. Cabrera-Palmer,[9] D. Chernyak,[7,*] E. Conley,[2] J. Daughhetee,[6] J. Detwiler,[10] K. Ding,[7] M. R. Durand,[10] Y. Efremenko,[4,6] S. R. Elliott,[11] L. Fabris,[6] M. Febbraro,[6] J. Galambos,[6] A. Gallo Rosso,[12] A. Galindo-Uribarri,[6,4] M. P. Green,[3,6,8] M. R. Heath,[6] S. Hedges,[2,3] D. Hoang,[13] M. Hughes,[14] E. Iverson,[6] T. Johnson,[2,3] A. Khromov,[1] A. Konovalov,[1,5] E. Kozlova,[1,5] A. Kumpan,[1] L. Li,[2,3] J. M. Link,[15] J. Liu,[7] K. Mann,[8] D. M. Markoff,[16,3] J. Mastroberti,[14] M. McIntyre,[17] P. E. Mueller,[6] J. Newby,[6] D. S. Parno,[13] S. I. Penttila,[6] D. Pershey,[2] R. Rapp,[13,†] H. Ray,[17] J. Raybern,[2] O. Razuvaeva,[1,5] D. Reyna,[9] G. C. Rich,[3] D. Rimal,[17] J. Ross,[16,3] D. Rudik,[1] J. Runge,[2,3] D. J. Salvat,[14] A. M. Salyapongse,[13] K. Scholberg,[2] A. Shakirov,[1] G. Simakov,[1,5] G. Sinev,[2,‡] W. M. Snow,[14] V. Sosnovstsev,[1] B. Suh,[14] R. Tayloe,[14] K. Tellez-Giron-Flores,[15] I. Tolstukhin,[14,§] S. Trotter,[6] E. Ujah,[16,3] J. Vanderwerp,[14] R. L. Varner,[6] C. J. Virtue,[12] G. Visser,[14] T. Wongjirad,[18] Y.-R. Yen,[13] J. Yoo,[19] C.-H. Yu,[6] J. Zettlemoyer,[14,‖] and S. Zhang[13,14]

(COHERENT Collaboration)

[1]*National Research Nuclear University MEPhI (Moscow Engineering Physics Institute), Moscow 115409, Russian Federation*
[2]*Department of Physics, Duke University, Durham, North Carolina 27708, USA*
[3]*Triangle Universities Nuclear Laboratory, Durham, North Carolina 27708, USA*
[4]*Department of Physics and Astronomy, University of Tennessee, Knoxville, Tennessee 37996, USA*
[5]*Institute for Theoretical and Experimental Physics named by A.I. Alikhanov of National Research Centre "Kurchatov Institute", Moscow 117218, Russian Federation*
[6]*Oak Ridge National Laboratory, Oak Ridge, Tennessee 37831, USA*
[7]*Physics Department, University of South Dakota, Vermillion, South Dakota 57069, USA*
[8]*Department of Physics, North Carolina State University, Raleigh, North Carolina 27695, USA*
[9]*Sandia National Laboratories, Livermore, California 94550, USA*
[10]*Center for Experimental Nuclear Physics and Astrophysics & Department of Physics, University of Washington, Seattle, Washington 98195, USA*
[11]*Los Alamos National Laboratory, Los Alamos, New Mexico 87545, USA*
[12]*Department of Physics, Laurentian University, Sudbury, Ontario P3E 2C6, Canada*
[13]*Department of Physics, Carnegie Mellon University, Pittsburgh, Pennsylvania 15213, USA*
[14]*Department of Physics, Indiana University, Bloomington, Indiana 47405, USA*
[15]*Center for Neutrino Physics, Virginia Tech, Blacksburg, Virginia 24061, USA*
[16]*Department of Mathematics and Physics, North Carolina Central University, Durham, North Carolina 27707, USA*
[17]*Department of Physics, University of Florida, Gainesville, Florida 32611, USA*
[18]*Department of Physics and Astronomy, Tufts University, Medford, Massachusetts 02155, USA*
[19]*Department of Physics and Astronomy, Seoul National University, Seoul 08826, Korea*

(Received 31 March 2022; accepted 7 July 2022; published 2 August 2022)

The Spallation Neutron Source (SNS) at Oak Ridge National Laboratory is a pulsed source of neutrons and, as a by-product of this operation, an intense source of pulsed neutrinos via stopped-pion decay. The COHERENT collaboration uses this source to investigate coherent elastic neutrino-nucleus scattering and

[*]Present address: Department of Physics and Astronomy, University of Alabama, Tuscaloosa, Alabama, 35487, USA and Institute for Nuclear Research of NASU, Kyiv, 03028, Ukraine.
[†]rrapp@andrew.cmu.edu
[‡]Present address: South Dakota School of Mines and Technology, Rapid City, South Dakota 57701, USA.
[§]Present address: Argonne National Laboratory, Argonne, Illinois 60439, USA.
[‖]Present address: Fermi National Accelerator Laboratory, Batavia, Illinois 60510, USA.

other physics with a suite of detectors. This work includes a description of our Geant4 simulation of neutrino production at the SNS and the flux calculation which informs the COHERENT studies. We estimate the uncertainty of this calculation at the ∼10% level based on validation against available low-energy π^+ production data.

DOI: 10.1103/PhysRevD.106.032003

I. INTRODUCTION

At the Spallation Neutron Source (SNS) at Oak Ridge National Laboratory (ORNL), a pulsed 1.4-MW beam of ∼1-GeV protons strikes an approximately 50 cm-long Hg target [1]. The incident protons interact multiple times within the thick target, losing energy and spalling nuclei to create the intended neutrons and by-product charged pions. The majority of the π^+ come to rest (less than 1% decay in flight) within the thick and dense target, and their stopped decays then give rise to neutrinos with energies of order tens of MeV:

$$\begin{aligned} \pi^+ &\to \mu^+ + \nu_\mu \\ \mu^+ &\to e^+ + \bar{\nu}_\mu + \nu_e. \end{aligned} \tag{1}$$

SNS interactions also produce copious quantities of π^-, but the vast majority (∼99%) of these capture on nuclei in the target before decaying and rarely produce neutrinos. The proton beam energy is too low to create substantial numbers of other neutrino-producing decay chains, such as those of $K^\pm$ or η.

To take advantage of this high-intensity pulsed-neutrino source, the COHERENT collaboration has deployed multiple neutrino detectors 20–30 m from the target in the SNS basement corridor known as "Neutrino Alley." The collaboration has performed the first-ever measurements of the cross section of coherent elastic neutrino-nucleus scattering (CEvNS) with the COH-CsI [2] and COH-Ar-10 detectors [3]. CEvNS measurements are planned on additional nuclear targets (Na and Ge), as well as measurements of several charged-current neutrino-interaction cross sections of interest to nuclear and particle physics and astrophysics [4]. As COHERENT's cross-section measurements become more precise, they will illuminate physics topics including nonstandard neutrino interactions [5,6], neutrino electromagnetic properties [7–11], nuclear form factors and neutron distributions [12–14], and the detection of supernova neutrinos by both dedicated observatories [15,16] and next-generation neutrino-oscillation experiments [17–19].

Precise knowledge of the SNS neutrino flux is essential to unlocking the full physics potential of the COHERENT cross-section measurements. The uncertainty on the overall normalization of the neutrino flux is the dominant systematic uncertainty in the Ar results [3] and the second-largest systematic in the initial CsI results [2]. Thanks to updated measurements of the quenching factor in CsI, the neutrino flux is the dominant systematic in the final CsI results [20].

We have built a detailed model of the SNS using the Geant4 Monte Carlo framework [21,22] to characterize the neutrino flux to the COHERENT detectors and have made it publicly available on Zenodo [23]. In addition to the geometry, the simulation accuracy relies on the underlying implementation of pion production in the Geant4 physics model. Section II describes our validation efforts using four standard physics lists against the available world π^+-production data. World data, however, are imperfect—Hg-target data are not available at low proton energies, data sets at proton energies near 1 GeV are very limited, and most pion-production cross sections are measured using thin targets that do not replicate the half-meter of dense material the protons at the SNS encounter. Although the existing data are insufficient for a precise validation, we estimate the uncertainty of our simulated flux with the QGSP_BERT physics list to be about 10%. Section III describes our simulation of the SNS, along with our tools for studying the characteristics of the resulting neutrinos. We also discuss the effect of changes to SNS operating conditions; for example, the incident proton kinetic energy has ranged from 0.83–1.011 GeV during COHERENT's lifetime in Neutrino Alley. Section IV summarizes the properties of our simulated neutrino flux using the selected physics list.

Our SNS simulation has applications to additional nuclear and particle physics experiments proposed at the SNS. In Sec. V, we present a neutrino-flux simulation based on preliminary design work for a proposed second target station (STS) with a tungsten target; our results suggest that the STS could be a very productive site for next-generation neutrino experiments. Section VI describes the use of our simulation to study π^0 and π^- production at the SNS, relevant to accelerator-based searches for light dark matter. We discuss several future avenues for reducing uncertainties related to the SNS neutrino flux in Sec. VII and conclude in Sec. VIII.

II. VALIDATION OF π^+-PRODUCTION MODELS

We investigated four standard physics models (or "physics lists") as implemented in Geant4.10.06.p01: FTFP_BERT, QGSP_BERT, QGSP_BIC, and QGSP_INCLXX. With all SNS protons well below 10 GeV, the differences in the underlying string models of FTFP_BERT and QGSP_BERT were found to be negligible; in this work, we focus only on

the QGSP models. We note here that the plots within this section use natural units, such that $c = 1$.

Each candidate for our physics list models nuclear structure in a specific way. With an implementation of the classical Bertini Cascade model [24] for incident hadrons below 3 GeV, QGSP_BERT is a favored model for the production of hadrons (and subsequently, neutrinos) with its treatment of the nucleus as a gas of nucleons that can be solved on average using the Boltzmann equation for a projectile moving through the gas [25]. The QGSP_BIC physics list differs only for protons and neutrons, for which it implements a binary cascade and models the nucleus as an isotropic sphere. In this model, the nucleons are placed at specific positions that projectiles can interact with individually, and each nucleon carries a random momentum between zero and the Fermi momentum [26]. Finally, QGSP_INCLXX extends the Liège Intranuclear Cascade model [27] benchmarked against spallation studies below 3 GeV [28] by modeling the nucleus in a very similar manner to QGSP_BIC, but adding the possibility to emit nucleon clusters that can cause secondary reactions after a projectile interacts with the nucleus. Both QGSP_BIC and QGSP_INCLXX require increased computation time (compared to QGSP_BERT) to model the interactions of projectiles with more massive nuclei [29].

In prior estimations the COHERENT collaboration has used the QGSP_BERT physics list with an assigned 10% uncertainty on any flux predictions coming from simulation efforts. This estimate was informed by prior studies using an implementation of the Bertini model in the LAHET Monte Carlo framework [30] to make predictions for the LSND and KARMEN experiments [31–33]. World data at the time of their investigation did not agree with LAHET predictions, and LAHET predictions that were renormalized to match available data were lower than Geant4 predictions [31,34,35]. The 10% systematic was assigned to our neutrino-flux calculations to conservatively account for this discrepancy [2].

Since the lack of pion-production data from 1 GeV proton-mercury interactions prevents a direct comparison, our choice of physics model must be validated via other targets, usually at higher energies. In Sec. II A, we compare the total π^+-production cross section to the Norbury-Townsend parametrization developed to match data from proton-nucleus and nucleus-nucleus collisions [36]. Not included in the development of the Norbury-Townsend parametrization, however, are newer results focusing on double-differential measurements, such as those from the thin-target HARP experiment [37]. We detail our validations against the HARP measurements in Sec. II B. Older experiments also collected double-differential pion-production data at energies closer to the SNS, such as Abaev *et al.* in 1989 [38], but their data have a very limited angular coverage. We use these data sets to check the model behavior at lower proton energies (Sec. II C) since they cannot constrain our total neutrino flux. We discuss the effects of modeling the thick target of the SNS in Sec. II D and interpret all of our validation work to estimate a neutrino flux systematic for COHERENT in Sec. II E.

A. Norbury-Townsend parametrization

The Norbury-Townsend parametrization is an empirical function developed to parametrize pion-production data from proton-nucleus and nucleus-nucleus interactions measured by Nagamiya *et al.* [39]. While developed in the right energy range for SNS operations at ∼1 GeV, π^+ production data were only taken for subsets of Ne + NaF, Ne + Cu, Ne + Pb, C + C, C + Pb, Ar + KCl, Ar + Pb for 0.4, 0.8, and 2.1 GeV per incident nucleon—only π^- production data were available from the proton-nucleus studies [36]. Although our focus is π^+ production in this work, we note that future effort to check the candidate physics models against the parametrizations for π^- and π^0 production will be useful to validate the flux predictions for dark-matter-producing particles at the SNS that, we present in Sec. VI.

The Norbury-Townsend parametrization of the π^+ production cross section (σ_{π^+} in mb) from incident protons is shown in Eq. (3), where A_t is the number of target nucleons, and E_i (in GeV) is the energy per incident nucleon [36]:

$$\sigma_{\pi^+} = \frac{A_t^{2.2/3}}{0.00717 + 0.0652\frac{\log(E_i)}{E_i} + \frac{0.162}{E_i^2}}. \tag{2}$$

This parametrization overpredicts the π^+-production from the Ar + Pb and Ne + Pb data used in the development by between 15% and 30%, though, we do note that this demonstrates a 1σ consistency due to the large errors of the datasets from the early 1980s.

Using a thin simulated target to minimize proton energy loss ($5 \times 5 \times 0.5$ cm^3) and specifying the isotope, molar mass, and density for each target, we counted the total number of pions produced. We then scaled this event rate by our simulated number of target nuclei and incident flux of protons to convert to a total cross-section prediction. Figure 1 shows comparisons of these results to the parametrization across incident energies (top) and target nucleus (bottom), with a 10% uncertainty applied to the cross sections from each potential physics list.

The top panel of Fig. 1 demonstrates that for p + Hg at 1 GeV, QGSP_BERT and QGSP_INCLXX agree with the parametrization at a ∼15% level, and generally have better agreement at lower energies (∼10% at 0.8 GeV) than at higher energies (∼25% at 1.3 GeV). The QGSP_BIC model, however, consistently overpredicts the p + Hg parametrization by more than 50% from 0.8–1.3 GeV. The bottom panel of Fig. 1 illustrates that for 1 GeV p + A, QGSP_BERT and QGSP_INCLXX agree with the parametrization at the ∼15% level for nuclear targets near Hg. Due to the high uncertainties in the parametrization and its

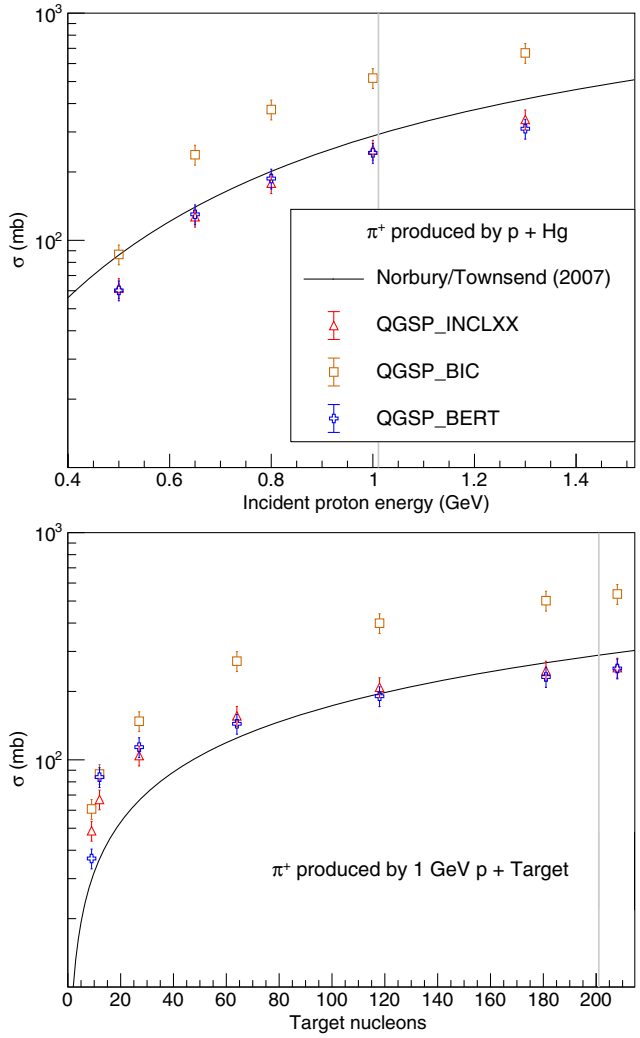

FIG. 1. Comparisons of the Norbury-Townsend parametrization and Geant4 model predictions of total pion-production cross section. Top: dependence of total cross section on incident proton energy for a mercury target. The vertical line indicates the current SNS operating energy of 1.011 GeV, but COHERENT still sees π^+ production at energies below this value due to proton energy loss within the thick target (see Fig. 16). Bottom: dependence of total cross section on target nucleus for a proton energy of 1 GeV. The vertical line represents a mercury target.

underlying datasets, we use these results to demonstrate a reasonable consistency at an ∼15% level for the predictions of both QGSP_BERT and QGSP_INCLXX, and to identify the overall normalization problem of QGSP_BIC.

B. HARP and HARP-CDP

HARP, the Hadron Production Experiment (PS214), operated at CERN's Proton Synchrotron from 2000 to 2002. With a nearly 4π acceptance and incident proton momentum range from 1.5 GeV/c to 15 GeV/c, HARP measured 7 different solid targets (Be, C, Al, Cu, Sn, Ta, Pb) as well as 4 cryogenic liquid targets (H_2, D_2, N_2, O_2). The HARP collaboration disagreed on their TPC calibrations causing a subgroup, HARP-CDP, to promote different calculations of pion momenta and identification of protons and pions [40]. Both of these differences impact the final analysis, such that HARP-CDP reports 16–34% lower integrated cross sections (shown in Fig. 4) than the HARP analysis, depending on the target. In this paper, both sets of cross-section results were checked against our Monte Carlo simulations.

Data were not collected for incident protons at 1 GeV; therefore, we compare to the HARP and HARP-CDP analyses of 3 GeV/c data on a large range of nucleon numbers: Be [41], C [42,43], Al [41,44], Cu [42], Sn [42,45], Ta [46,47], and Pb [41,48]. We follow a similar procedure to our Norbury-Townsend comparisons and simulate monoenergetic protons with 2.205 GeV of kinetic energy (calculated from the 3 GeV/c beam momentum) incident on a thin target ($5 \times 5 \times 0.5$ cm^3), though here counting pions produced per pion momentum and production angle rather than total number of pions. We then scale the stored event rates by our simulated target details to convert to a doubly differential cross-section prediction from each simulation model. Figure 2 illustrates the direct comparison of our simulation to the HARP and HARP-CDP results for 3 GeV/c p + ^{208}Pb. The simulation error bands combine statistical uncertainty with the estimated 10% systematic uncertainty on the simulation prediction. The HARP and HARP-CDP data consistently disagree with the simulation predictions by more than 10% in the low-angle bins, but generally start to demonstrate consistency with QGSP_BERT and QGSP_INCLXX in the higher-angle bins. We also note that the simulation generally better-predicts the data in the higher-momentum bins, and the normalization problem of QGSP_BIC is evident in the low-momentum bins.

Since the Geant4 models predict the HARP and HARP-CDP data better in some bins than others and the SNS neutrino flux is known to arise from π^+ decay at rest (see Table II), we integrate away the angular or momentum dependence to compare singly differential cross sections. The comparisons shown in Fig. 3 integrate our simulation prediction over the angular region of the HARP analysis; there is less than a 1% difference from the simulation prediction integrated over the HARP angular region and over the HARP-CDP angular region, so we show HARP-CDP data on the same axes.

The SNS mercury target is thick and dense enough to stop the majority of the pions regardless of production angle or momentum. Therefore, to a very good approximation, we require only the total cross section to simulate the neutrino production. We integrate away the dependence on both production angle (350–2150 mrad) and momentum (0.1–0.8 GeV) and show the total cross-section comparisons to both HARP and HARP-CDP data in Fig. 4. The ratio of the Geant4 model prediction to the HARP or

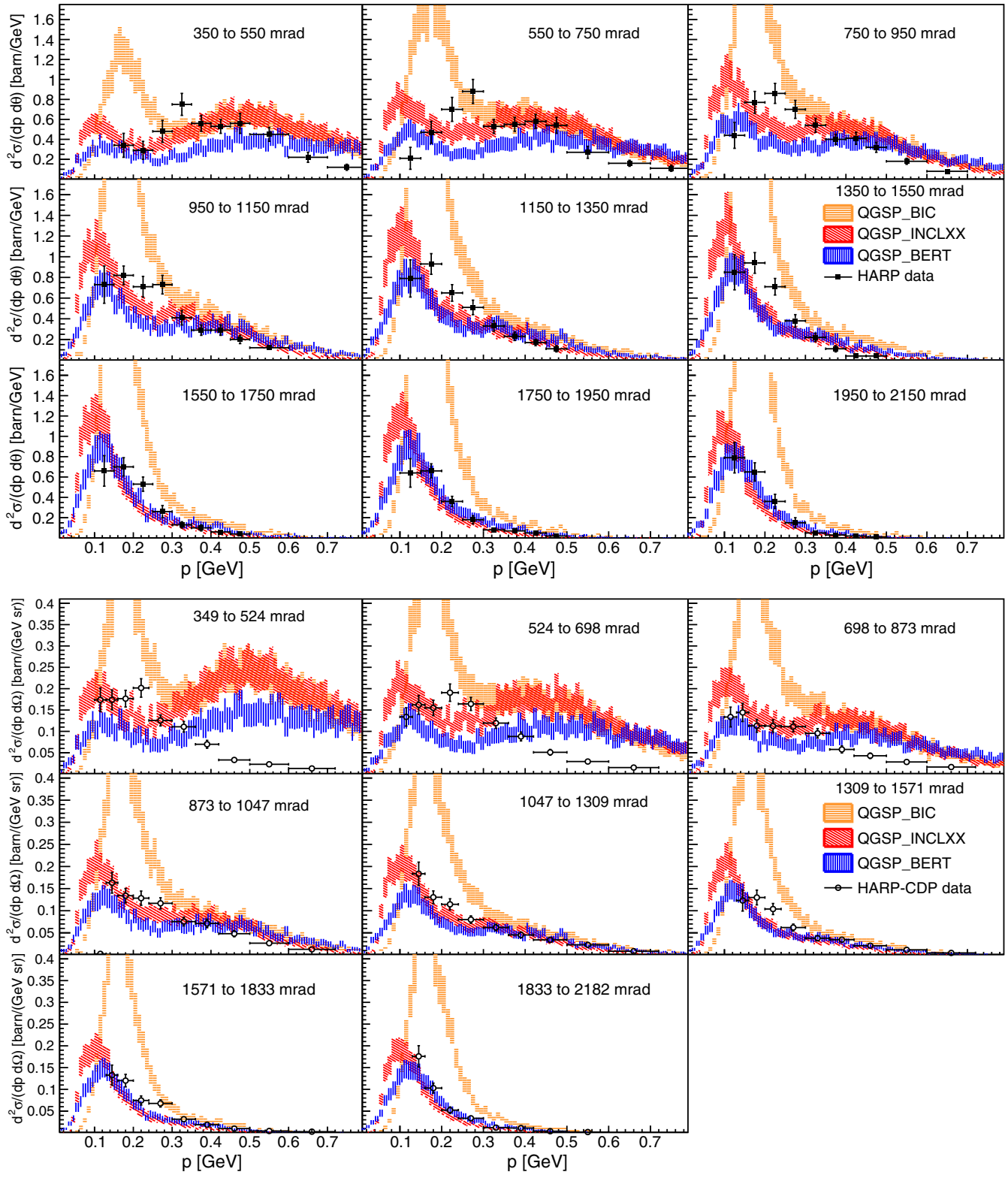

FIG. 2. Comparisons of double-differential cross sections of π^+ production from 3 GeV/c p + ^{208}Pb as predicted by the different Geant4 physics lists to the measurements from HARP (top) and HARP-CDP (bottom). The error band shown for each physics list is a 10% uncertainty. We highlight ^{208}Pb because, among HARP targets, this isotope is closest in mass to the SNS mercury target.

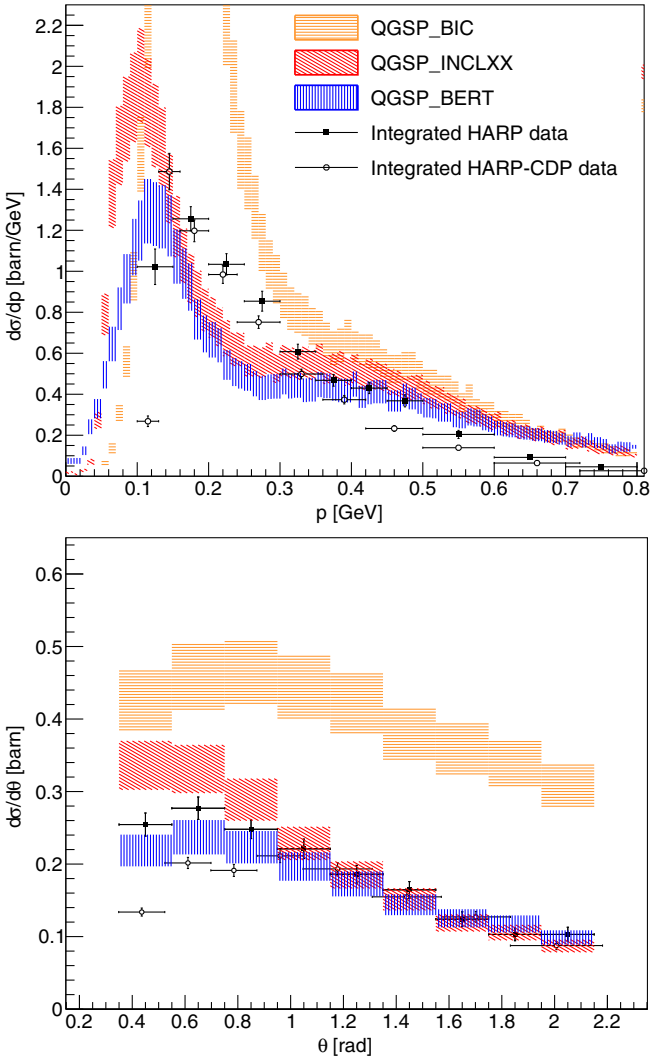

FIG. 3. Comparison of measured differential cross sections of π^+ production from 3 GeV/c p + ^{208}Pb to Geant4 physics lists. Top: HARP and HARP-CDP data were integrated over their respective angular regions and compared to simulation integrated from 350 to 2150 mrad in production angle. Bottom: HARP and HARP-CDP data were integrated from 0.1 to 0.8 GeV/c in momentum and compared to simulation integrated on the same region.

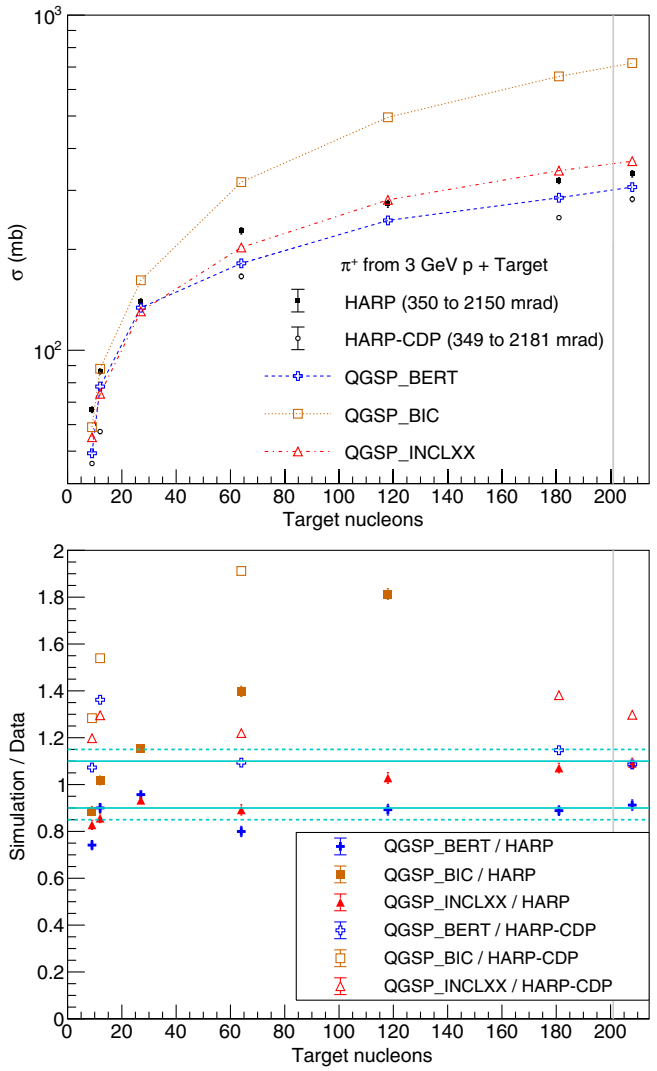

FIG. 4. Top: the HARP data and Geant4 model predictions of the pion-production cross section integrated over 350–2150 mrad and 0.1–0.8 GeV. The HARP-CDP data are also shown but are integrated over 349–2181 mrad and 0.1–0.8 GeV. Bottom: ratio of the Geant4 simulated predictions to the central values of the data, plotted with an uncertainty on all three simulations shown as data error/central value (the HARP-CDP error bars are small enough to be hidden by the points themselves). The horizontal solid cyan lines mark a $\pm 10\%$ 1σ uncertainty band, and the dashed cyan lines mark a $\pm 15\%$ 1σ uncertainty band. The vertical gray line on each plot represents a mercury target.

HARP-CDP result determines how well we predict the data and is therefore considered in this work as the most convincing estimate of our systematic uncertainty (more in Sec. II E).

C. Low-energy pion-production data

Using the proton synchrotron at the Leningrad Nuclear Physics Institute (Gatchina, Russia) with a beam kinetic energy of 997 ± 5 MeV, Abaev *et al.* measured pion production on 16 different targets (isotopes of H, B, C, O, Mg, Al, Cu, Sn, Ta, W, and Pb) at 0° and 57.8° with 0.01 steradian angular acceptance [38]. We compare to a range of nucleon numbers, but we exclude comparisons to different isotopes of the same nucleus in this work as no significant difference between different isotopes was found in the cross sections from data or simulation. The double-differential comparisons of the Geant4 models to Abaev *et al.* are shown in Fig. 5, and the momentum-integrated comparisons are shown in Fig. 6.

The bottom panel of Fig. 5 at 57.8° (∼1009 mrad) is similar to the center-left panels of the HARP (950–1150 mrad) and HARP-CDP (873–1047 mrad) results shown in Fig. 2,

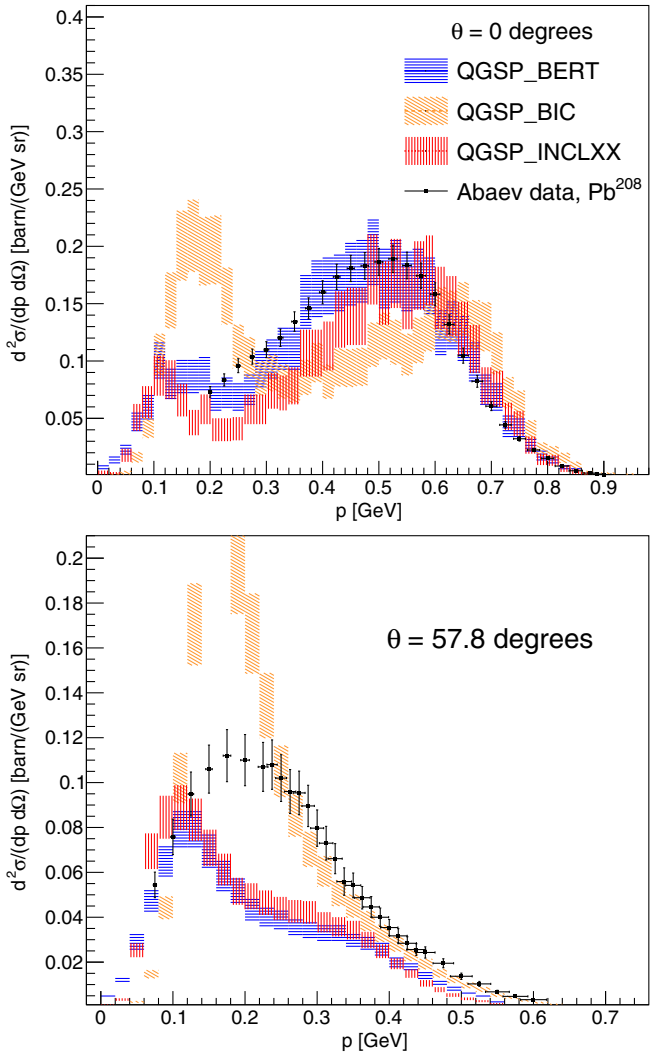

FIG. 5. Comparisons of double-differential cross sections of π^+ production from 1 GeV p + ^{208}Pb at 0° and 57.8° as predicted by the different Geant4 physics lists to the measurements from Abaev *et al.* [38].

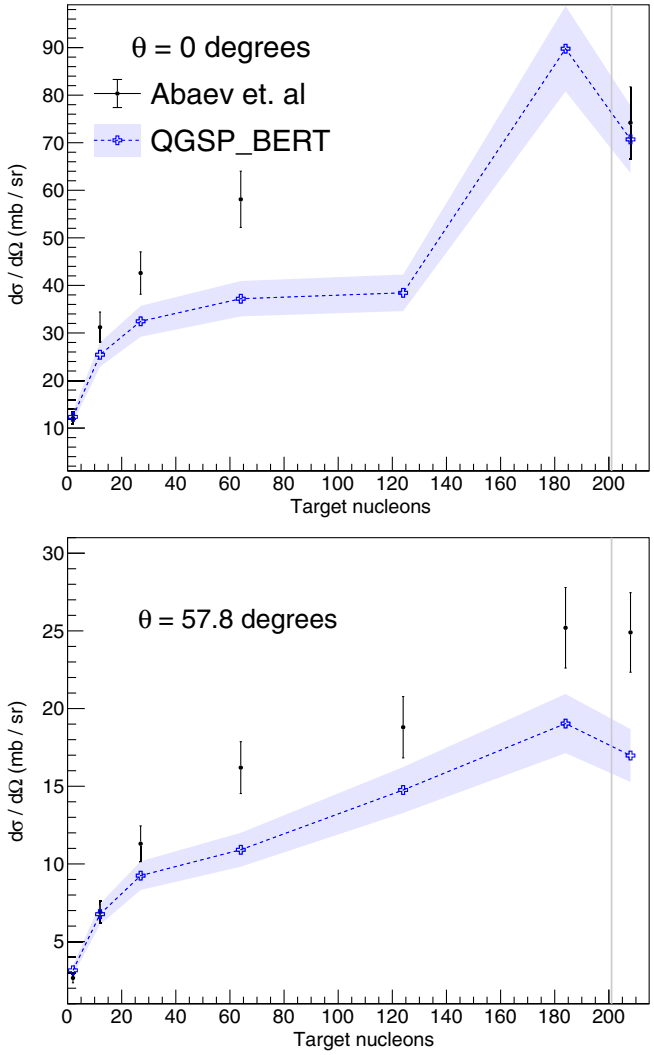

FIG. 6. Comparisons of differential cross sections at 0° and 57.8° as predicted by QGSP_BERT to measurements by Abaev *et al.* [38]. The vertical gray lines represent a mercury target.

albeit with different incident proton energy and angular acceptance. We observe a similar disagreement with the double-differential comparisons, but a slightly better agreement with the momentum-integrated comparison in Fig. 6. The points at 208 nucleons in the momentum-integrated comparisons of Fig. 6 are similar to the behavior of a single bin in the bottom panel of Fig. 3, albeit with larger angular acceptance. We observe that single angular bins do disagree with the HARP and HARP-CDP data by greater than 10%, which suggests that we cannot draw conclusions about the uncertainty on the total pion production from the limited angle coverage of the Abaev data. Focusing specifically on the comparisons to ^{208}Pb and noting that the 0° prediction of QGSP_BERT is consistent with the Abaev data at the 10% level, we infer that the 10% uncertainty consistent with HARP predictions is a reasonable estimate at lower proton energy.

D. Secondary particle interactions

The pion-production model of QGSP_BERT has the best agreement for thin-target data, but we must also model the proton energy loss and the interactions of any secondary particles that are produced. For example, π^+ scattering will affect our predictions on how many π^+ decay at rest, and pion interactions such as charge exchange or absorption will impact the number of π^+ that decay into neutrinos. We do not perform any specific validation of these processes in this work, but we offer some comments here about the models we implement.

Proton energy-loss models are important in Geant4, as they have broad applications within both the particle physics and medical communities. As a result, these models have undergone extensive validation efforts [49,50]. The energy-loss profile of protons is generally accurate to within 2% above 1 MeV. We do not perform

any further validation of the energy losses within the SNS target, and we neglect any uncertainty from the proton energy-loss profile within the thick SNS target in this work.

Pions and other secondary hadrons created at the SNS are well below 10 GeV and are simulated using the default cross-section tables implemented in the Bertini Cascade model (primarily the Baranshenkov and Glauber-Gribov parametrizations) [24]. In our simulations of the SNS, ~25% of the π^+ tracks that are produced end in nondecay processes (labeled "pi + Inelastic" in Geant4). There is less than a 1% difference between this fraction of nondecay destruction of pion tracks between QGSP_BERT and QGSP_INCLXX, though QGSP_BIC simulations estimate that nearer to 30% of π^+ tracks end in nondecay processes. A small fraction (less than 15%) of these "pi + Inelastic" track deaths can still result in neutrino production due to the production of additional protons or pions. We do not perform any specific validation of these processes in this work, and we neglect the uncertainty here given the difference between the QGSP_BERT and QGSP_INCLXX predictions and the previously identified normalization problem of the QGSP_BIC predictions.

E. Discussion

We are not aware of any data from p + Hg and very few data sets exist at these energies, so this work is intended as a cross-check of prior estimates rather than as a derivation of our neutrino-flux systematic while new experimental efforts are developed (see Sec. VII). We find that QGSP_BERT is the only model which agrees at the 10% level with the cross section measurements of both HARP and HARP-CDP for the ^{208}Pb dataset (the closest to Hg); the other lists overpredict the HARP-CDP data. For lighter nuclei like W (see Sec. V), these comparisons suggest that a 15% uncertainty on the QGSP_BERT prediction would be more appropriate. The comparison against the Norbury-Townsend parametrization shows reasonable consistency at the 10% level with QGSP_BERT and QGSP_INCLXX, and further demonstrates an overall normalization problem with QGSP_BIC, despite noteworthy agreement in the tails of the 57.8° Abaev measurement. While QGSP_INCLXX is acceptable, QGSP_BERT has better agreement with the data and the added bonus of being more computationally efficient since QGSP_INCLXX produces energy conservation errors in some of the SNS volumes. We note that while the momentum-integrated Abaev data may disagree with QGSP_BERT predictions at more than the 10% level, similar disagreement is shown in the bottom panel of Fig. 3 for single points of the momentum-integrated HARP and HARP-CDP comparisons; it is only after an additional integration over angle that good agreement is achieved. Ultimately, the limited angular coverage of the Abaev data limits our ability to investigate this effect.

In light of these studies and prior work using the Bertini cascade for neutrino flux calculations [31–33,51,52], we choose to use QGSP_BERT with a 10% uncertainty on the flux predictions that come from our Geant4 simulations. This systematic uncertainty needs to be reduced for the future precision program of COHERENT, and we describe future avenues for experimentally reducing this uncertainty in Sec. VII.

III. MODELING THE SPALLATION NEUTRON SOURCE IN GEANT4

The design of the SNS target and moderator suite was optimized for neutron production and related science [1]. We define simplified components of the SNS target monolith that are expected to contribute to pion production or to the stopping of pions and muons. The simplification process is demonstrated in the top panel of Fig. 7, where the

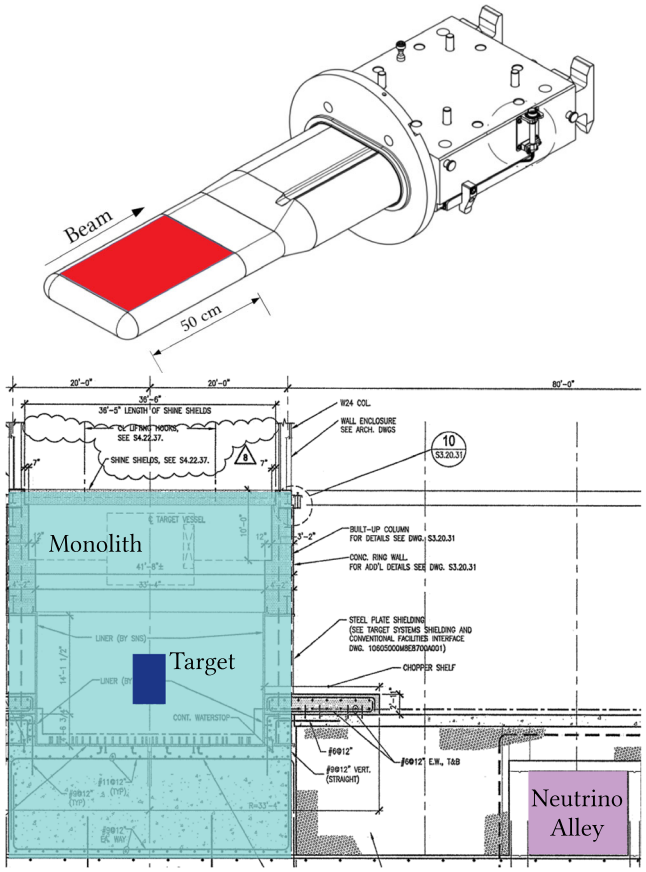

FIG. 7. Top: ORNL technical drawing of the target vessel. The red section highlights the main Hg target as implemented in our Geant4 model. Bottom: A portion of an ORNL technical drawing illustrating the target hall, with pieces in our Geant4 model highlighted. The outer shaded cyan is the concrete monolith, with the inner indigo representing the steel containing the Hg target and moderators. In the bottom right corner, the shaded purple shows the location of Neutrino Alley relative to the target monolith [53].

TABLE I. An overview of components in our Geant4 model that contribute to the overall pion-production. We also include the fraction of π^+, and therefore ν, our simulations produce as a result of each volume. We report the dimensions from the perspective of the beamline as either Width × Height × Depth or Diameter (∅) × Height. The depth of the Inconel proton beam window (PBW) is an approximation (indicated by an *) of 3 cm, which includes some amount of vacuum immediately before and after the window as a result of the curvature.

			π^+ contributed	
Component	Material	Dimensions	Aluminum PBW (%)	Inconel PBW (%)
Target	Hg	$39.9 \times 10.4 \times 50.0$ cm^3	94.12	(90.91)
Target casing	Steel	$40.9 \times 11.4 \times 51.0$ cm^3	0.20	(0.56)
Inner plug (2)	Be, D_2O	70.0 cm ∅, 45 cm	0.19	(0.23)
Moderator (4)	H_2 (3), H_2O (1)	$4.0 \times 13.9 \times 17.1$ cm^3	0.01	(0.01)
Reflector	Steel, D_2O	108 cm ∅, 101.6 cm	0.99	(1.34)
Beamline shielding	Steel	$64.8 \times 54.6 \times 200.0$ cm^3	0.93	(1.72)
Target room	Steel	1002 cm ∅, 950.8 cm	0.00	(0.14)
Aluminum PBW	Al-6061, H_2O	$29.8 \times 14.6 \times 0.02$ cm^3	2.77	(…)
Aluminum beamline	Air	$29.8 \times 14.6 \times 200.0$ cm^3	0.79	(…)
Inconel PBW	Inconel-718, H_2O	$26.7 \times 12.7 \times 3.0$ cm^3*	…	(4.32)
Inconel beamline	Air	$26.7 \times 12.7 \times 200.0$ cm^3	…	(0.77)

technicalities of the target vessel are reduced to the mercury-containing region shaded red. The bottom panel of Fig. 7 highlights the target monolith and Neutrino Alley to illustrate the structures we build into our model. The details of our SNS model, along with their relative contributions to the overall π^+ production, are shown in Table I, and the full visualization of our simple model is shown in Fig. 8.

Though most of the components, we simulate are essentially unchanged during running despite routine maintenance and possible replacements, we must carefully consider the proton beam window (PBW) separating the vacuum of the accelerator from the target. Each proton must pass through the PBW, resulting in both proton energy loss and pion production as a result of interactions in the thin window. The PBW is routinely replaced due to radiation damage, and two different PBW designs have been in use during COHERENT's live-time in Neutrino Alley. A two-layered film design using Inconel, a nickel-based alloy trademarked by the Special Metals Corporation [54], with water cooling between the films, was used from the initial SNS production runs until January 11, 2017. An aluminum plate design with 50 drilled pipes for water cooling was in place until the latest replacement reverted back to an Inconel PBW on April 7, 2020. Figure 9 illustrates both PBW designs as modeled in our Geant4 geometry.

The SNS accelerates protons into an accumulator ring, which ensures that a focused beam of monoenergetic protons is directed on to the target. This beam is magnetically spread to prevent overheating of the proton beam window and target casing [55]; we introduce a uniformly distributed source using a prior measurement of the beam profile at the target [56] to account for this. Our simulated profile is illustrated in the bottom panel of Fig. 9 to show its size relative to the beam-window designs and target.

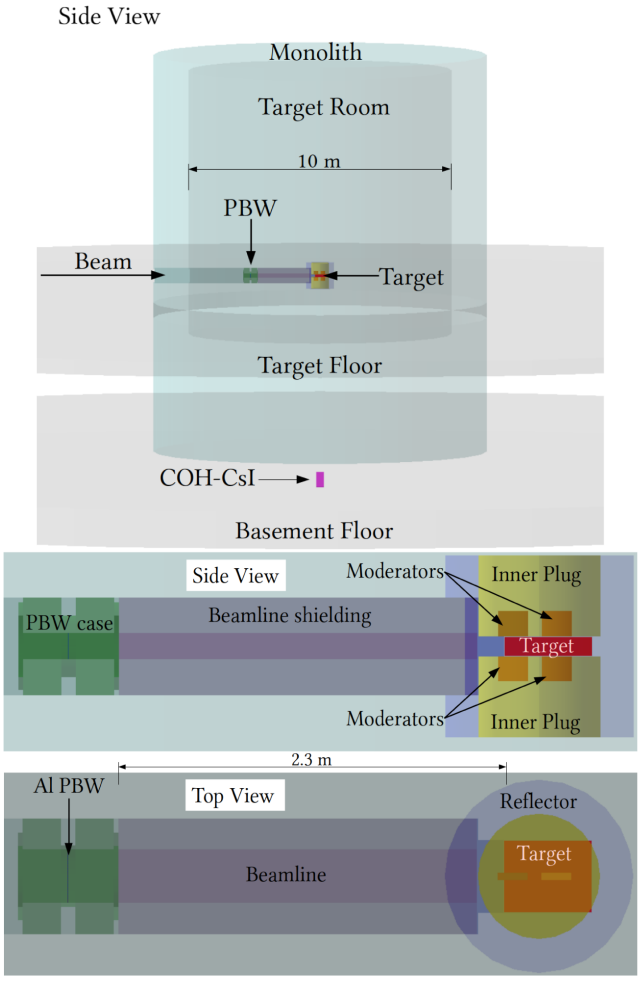

FIG. 8. Our Geant4 model of the SNS, simplified from ORNL technical drawings. Top: the full Geant4 world, highlighting the monolith relative to the location of COH-CsI in Neutrino Alley. Bottom: a view inside the outer monolith illustrating the target, neutron moderator suite, proton beam window, and beamline shielding.

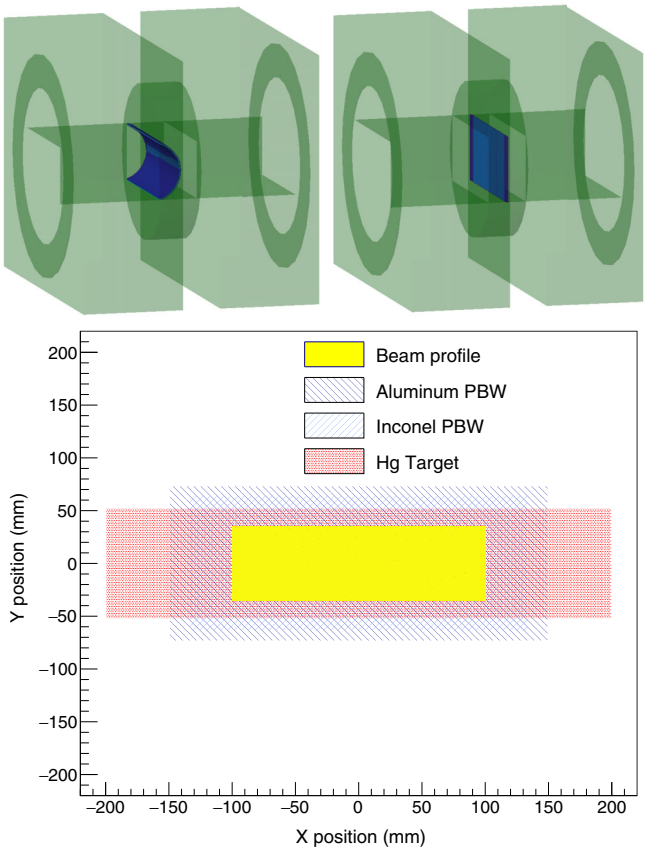

FIG. 9. Top left: Geant4 mockup of the dual-film Inconel PBW, with water cooling between the two films. Top right: Geant4 mockup of the aluminum plate PBW, with 50 vertical pipes for water cooling. Bottom: the position of incident protons shown relative to the profiles of the different PBW designs and Hg target.

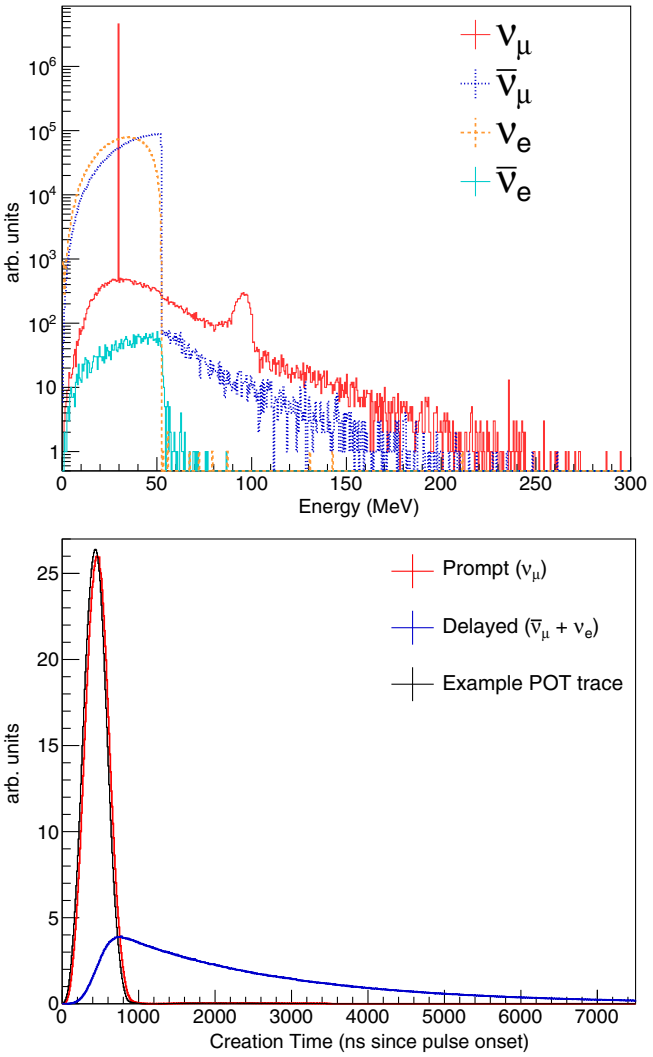

FIG. 10. Distributions of neutrino energy (top) and creation time (bottom) produced at the SNS, using QGSP_BERT to model the interactions of 1 GeV protons incident on the aluminum PBW geometry. We convolve the single-proton output of our simulations with the proton-on-target trace.

We specify the particles for the simulation to track, typically ν_x, $\pi^\pm$, $\mu^\pm$, $K^\pm$, η, p, and n, to ensure that we do not truncate any possible neutrino-production chain. Using the Monte Carlo framework of Geant4 and the QGSP_BERT physics model chosen in Sec. II, we observe which particles and interactions are responsible for generating the SNS neutrino flux. The predictions we make are dependent on our chosen physics model; for example, the QGSP_BIC nuclear model predicts some production of the η meson given 1 GeV incident protons, while other models do not.

IV. SIMULATED NEUTRINO FLUX FOR THE FIRST TARGET STATION

Figure 10 shows the energy and timing spectra for each neutrino flavor present in the simulation using the QGSP_BERT physics list to simulate incident protons with 1 GeV of kinetic energy on the SNS geometry with an aluminum PBW. We find that the SNS ν flux predictably demonstrates the characteristics of a pion decay-at-rest source such as the monoenergetic ν_μ at ~30 MeV from π^+ decay at rest and $\bar{\nu}_\mu$ and ν_e following the Michel spectra predicted from the three-body μ^+ decay at rest (DAR). Variations from these spectra include decays in flight (DIF), decays in orbit (DIO), and μ^- capture. We also observe some contribution from decay-at-rest kaons, notably in the ν_μ spectrum at ~240 MeV, but due to the small phase space available to produce these more massive particles, kaons have an almost negligible contribution to the SNS neutrino flux. Ultimately, this simulation predicts a decay-at-rest neutrino source with greater than 99% purity, with the exact creation process and parent particle breakdown shown for the aluminum PBW in Table II.

Using 1 GeV protons incident on our SNS geometry from behind the PBW, our simulations predict 0.262 neutrinos per proton on target. We find that our model of the SNS neutrino flux is primarily comprised of ν_μ, $\bar{\nu}_\mu$,

TABLE II. A breakdown of the processes and parent particles which create neutrinos for 1 GeV protons at the SNS with an aluminum PBW. The creation processes are classified as decay at rest (DAR), decay in flight (DIF), μ^- capture, or decay in orbit (DIO). We include significant figures here to sum to 100% given the small contributions outside of the π^+ DAR chain.

		Creation process				Parent particle		
	ν/POT	DAR (%)	DIF (%)	μ^- Cap (%)	μ^- DIO (%)	π^+ or μ^+ (%)	π^- or μ^- (%)	K^+ (%)
ν_μ	0.0875	98.940	0.779	0.196	0.084	99.7185	0.2812	0.0003
$\bar{\nu}_\mu$	0.0875	99.718	0.282	…	…	99.7187	0.2813	…
ν_e	0.0872	99.999	0.001	…	…	99.9999	…	0.0001
$\bar{\nu}_e$	0.0001	…	0.331	…	99.669%	…	100	…

and ν_e (each greater than $0.087\,\nu_X$/POT, where $X = \mu, \bar{\mu}, e$) with a small contribution of $\bar{\nu}_e$ ($0.0001\,\bar{\nu}_e$/POT, not considering the activation of materials near the target). We also see a small flux of low-energy $\bar{\nu}_e$ from neutron β-decay that we neglect in this work, with the intention of performing a dedicated study of radioactive products produced as a result of SNS operations in the future.

COHERENT deployed detectors at the SNS prior to the accelerator systems reaching 1 GeV, so data taken at lower energies (∼850 MeV) must also be understood. The upcoming Proton Power Upgrade [57] will prepare the SNS for the planned Second Target Station (described in Sec. V) by improving the accelerator. The upgrade will see the SNS operate at a more intense 2.0 MW, with 1.3 GeV incident protons by 2024. We use this simulation to study the dependence of the neutrinos produced on the incident proton energy and to develop an approach to account for changes to SNS operations over a run period. Figure 11 shows the energy dependence for both the total neutrino production and the fraction of neutrinos produced by the π^+ decay chain. We parametrize this dependence with cubic and linear fits, respectively, to develop a method for quickly estimating changes in the SNS neutrino production due to operational changes in the beam energy, and the parameters for each of the fits are listed in Table III. This figure also demonstrates that while there are minimal differences in total neutrino production between the two PBW designs, the differences in the relative contribution of pion production resulting from interactions with the PBW (see Table I) can impact the fraction of pions that will be brought to rest within the SNS target. The neutrino luminosity from the SNS given particular operating conditions can then be calculated as

$$\frac{\nu}{t} = \frac{\nu}{\mathrm{POT}}\frac{\mathrm{POT}}{t} = \frac{\nu}{\mathrm{POT}}\frac{E_{\mathrm{total}}}{E}\frac{1}{t} = F(E)\frac{P}{E}, \tag{3}$$

where E is the kinetic energy per proton, $F(E)$ is the fraction of ν produced per proton on target with incident kinetic energy E, E_{total} is the combined energy of all protons incident on the target in time t, and P is the SNS beam power (E_{total}/t). Figure 11 demonstrates that $F(E)$ can be estimated as a cubic polynomial in E with parameters defined in Table III, for E between 0.775 and 1.425 GeV. Plugging this into Eq. (3), we find a general parametrization for the SNS neutrino luminosity:

$$\frac{\nu}{t} = P\left(p_3E^2 + p_2E + p_1 + \frac{p_0}{E}\right). \tag{4}$$

Using this functional form and typical pre-upgrade operational parameters of 1.4 MW (7.0 GWhr/yr) and incident protons with 1 GeV of kinetic energy, we calculate 2.36×10^{15} neutrinos produced per second while the SNS is running. Estimating this production as an isotropic point source, we calculate a neutrino flux of $4.7 \times 10^7\ \nu\,\mathrm{cm}^{-2}\,\mathrm{s}^{-1}$ at 20 meters from the target center (the approximate location of the first CEvNS measurements in COH-CsI). Using the nominal SNS running time of 5000 hours per year, the SNS sees 1.58×10^{23} POT per year, with a ν luminosity of $4.25 \times 10^{22}\ \nu$ per year, or a flux of $8.46 \times 10^{14}\ \nu\,\mathrm{cm}^{-2}\,\mathrm{yr}^{-1}$ at 20 m from the target.

We also study the creation positions and momenta of the neutrinos, shown in Fig. 12. The volumes and materials which create the pions were listed in Table I; the neutrinos are primarily produced after the short movements of pions and muons coming to rest. The spread of the beam and the movements of the particles result in a radial spread from the beamline axis. Over 86% of the neutrinos are produced within 10 cm of the beamline axis, and almost all production (> 99%) occurs within 0.5 m of the beamline axis. Along the beamline axis, we find that over 90% of the neutrino production occurs within the target and less than 5% of the neutrinos are produced at the PBW location 2.5 m upstream of the target. Because the π^+ and μ^+ decay at rest, we also have almost fully isotropic production of neutrinos up to about 50 MeV. We do note visible anisotropy in the bottom panel of Fig. 12 for $E_\nu > 60$ MeV that is consistent with neutrinos boosted in the forward direction from pions decaying in flight.

We find that both PBW designs cause some neutrino production outside of the target regardless of the incident proton energy as illustrated in Fig. 13. However, our detectors are deployed ∼20 m from the target center, with the PBW placement only 2.5 m upstream of the target. To quantify the effect of this nonpointlike neutrino production,

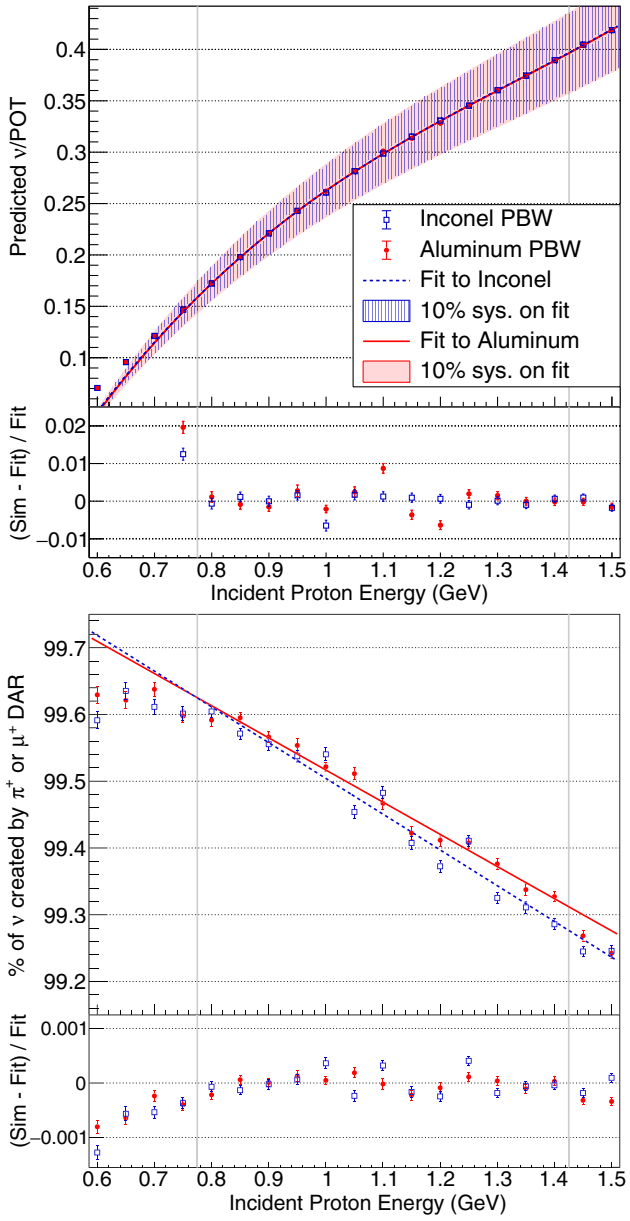

FIG. 11. Top: the total neutrino flux from the SNS will depend on the incident proton energy, and each operational configuration demonstrates a cubic dependence on this parameter. Bottom: the fraction of neutrinos produced from decay-at-rest processes demonstrates a linear dependence on the incident proton energy above ∼0.8 GeV. The fit range for both plots is $E \in [0.775, 1.425]$ GeV; this is the region between the vertical gray lines. The bottom panel in each plot shows the relative residuals, calculated as in the axis label from the simulation ("Sim") and fit ("Fit") predictions.

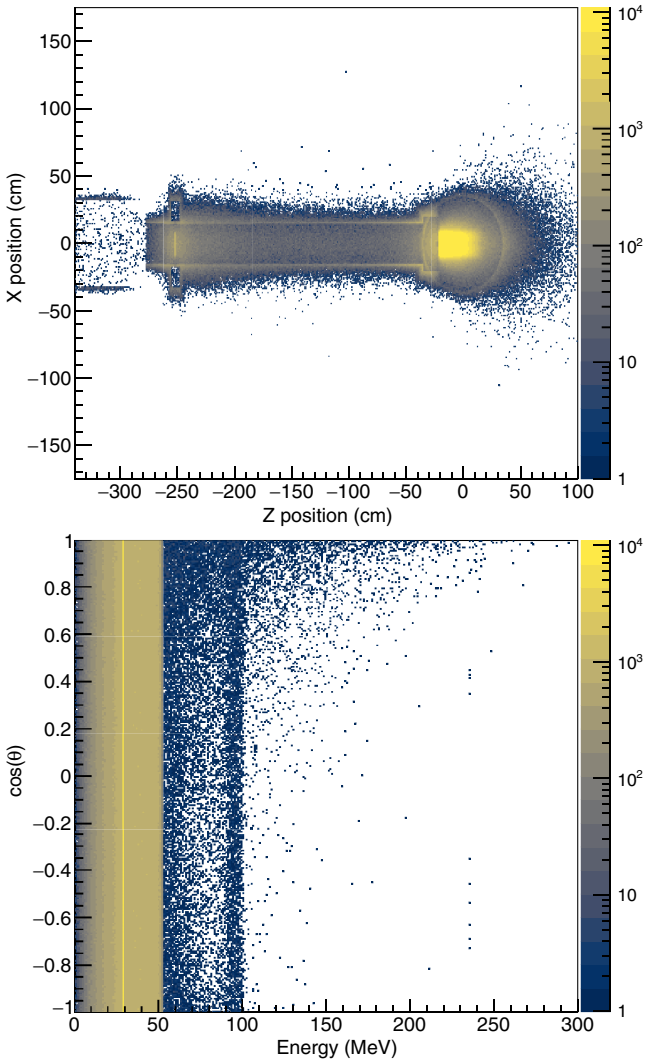

FIG. 12. Top: a top-down view of the neutrino creation positions. Bottom: distribution of the kinetic energies and production angles (relative to the beamline axis without convolving the creation-position information from the top panel) of all neutrinos.

we project the neutrino flux onto a 20 m sphere centered on the Hg target and determine an effective production angle based on the neutrino's projected location. In this model, the total anisotropy of the SNS neutrino flux 20 m from the target center is ∼5%. The dominant contribution is an excess near $\cos\theta \approx -1$ consistent with neutrino production within the PBW, with a secondary excess near $\cos\theta \approx 1$

TABLE III. Fit parameters for the proton-energy-dependence studies using both beam window designs. The three parameters for the cubic fits used in Eq. (3) ($F(E) = p_3E^3 + p_2E^2 + p_1E + p_0$) are illustrated in the top panel in Fig. 11, while the two parameters for the linear fits ($mE + b$) are illustrated in the bottom panel. The fit uncertainties do not consider the overall 10% systematic.

Design	p_3 (GeV^{-3})	p_2 (GeV^{-2})	p_1 (GeV^{-1})	p_0	b	m (GeV^{-1})
Aluminum PBW	0.28(2)	−1.12(6)	1.79(6)	−0.68(2)	99.99(1)	−0.48(1)
Inconel PBW	0.27(2)	−1.09(6)	1.75(6)	−0.67(2)	100.04(1)	−0.53(1)

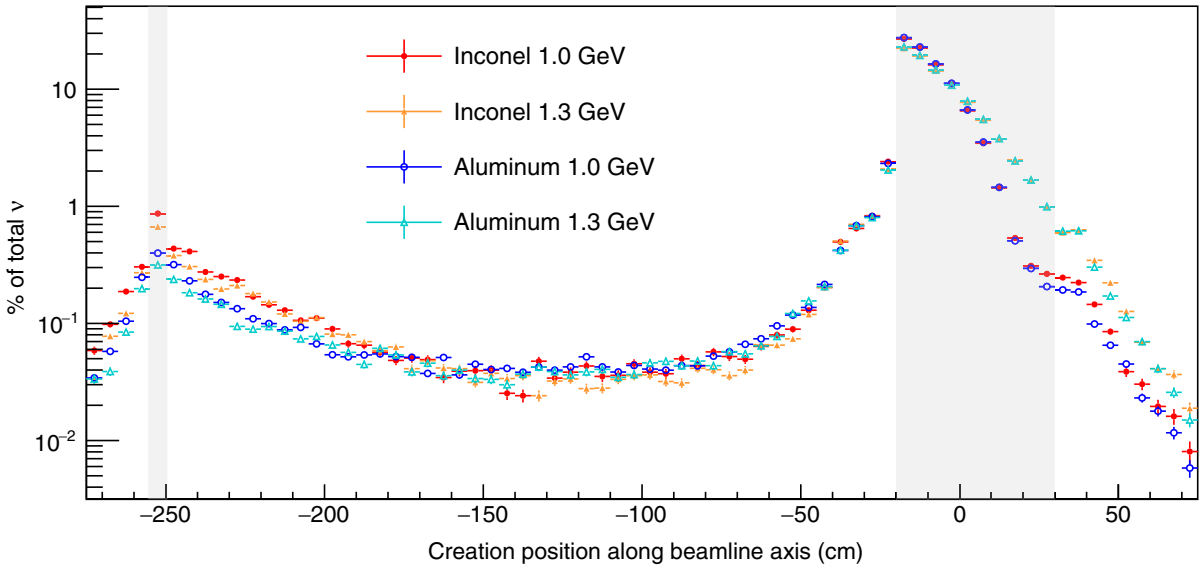

FIG. 13. A comparison of neutrino production along the beamline for different SNS configurations and beam energies. The gray shading to the left indicates the position of the proton beam window, and the shading to the right indicates the position of the Hg target.

consistent with neutrinos produced by decays in flight. For a small detector at the COH-CsI location 19.3 m from the target center and at $\cos\theta \approx 0$, we predict less than a 1% deficit of the neutrino flux compared to the isotropic point-source approximation. The contributions to the neutrino flux error from geometric considerations are small, and add negligibly in quadrature to the 10% uncertainty on the overall neutrino flux incident on our detectors in neutrino alley. The anisotropy depends on the relative contributions of the different materials in our SNS geometry outlined in Table I, and emphasizes the need for new pion-production measurements such as those discussed in Sec. VII.

V. NEUTRINOS AT THE SECOND TARGET STATION

We also created a model geometry to estimate the neutrino production at ORNL's planned Second Target Station (STS) [58]. With a projected completion in the early 2030s, COHERENT is engaged with the design phase of this facility to optimize location and shielding with the aim to deploy 10-ton-scale detectors for CEvNS and other physics. Using preliminary details about the planned target provided at the Workshop on Fundamental Physics at the Second Target Station in 2019 [59], we modeled 21 tungsten wedges surrounded by thin layers of tantalum and water, evenly spaced in an assembly with a 1.1 m diameter. We also modeled neutron moderators above and below the active target wedge, centered along the beamline axis. We simulated a 6 cm(width) × 5 cm(height) beam profile to ensure that the profile is smaller than that of a single tungsten wedge and included the aluminum PBW and beamline shielding as implemented in our First Target Station (FTS) geometry. This target geometry is illustrated in Fig. 14 and is centered inside a 5 m vacuum box, then enclosed in a steel box (10 m outer edge, 5 m inner) to mimic pion production in typical shielding materials without assuming specific geometry for the STS target surroundings.

With this simple geometry and 1.3 GeV incident protons, our simulations predict 0.13 ν_X/POT for ν_μ, $\bar{\nu}_\mu$, and ν_e from the π^+ decay chain, resulting in an approximate total 0.39 ν/POT. This estimate is larger than the predictions for the FTS operating at 1.3 GeV due to the increased density of a solid tungsten target. We cannot accurately discuss the decay-at-rest fraction of neutrinos or relative impact of the PBW since the shielding surrounding the target remains unknown. However, we note that protons do escape the end of the 25-cm thick active target wedge with enough energy that nearly 10% of the simulated pion production in our simple geometry occurs downstream of the target.

The STS will receive one of every four pulses from the SNS linear accelerator and will operate as a 15 Hz, 0.8 MW

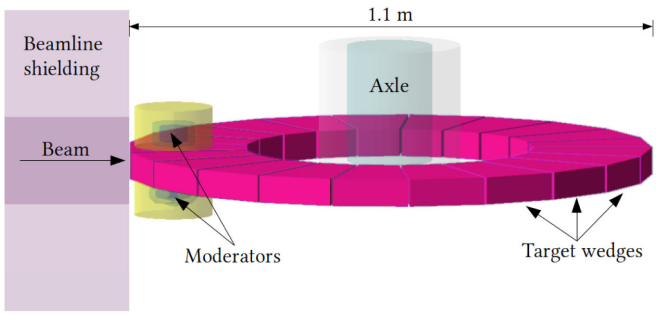

FIG. 14. Geant4 implementation of the Second Target Station target and moderators.

facility. Possible locations for 10-ton scale COHERENT detectors at the Second Target Station have been identified within a few tens of meters from the planned target location [60]. With a tungsten target rather than mercury, the uncertainty on the overall pion production is expected to be nearer to 15% (see bottom panel of Fig. 4), though efforts to normalize the neutrino flux at the FTS using D_2O and new hadron production experiments using a range of targets at lower beam energies will help to constrain our predictions (see Sec. VII).

VI. LIGHT DARK-MATTER PRODUCTION AT THE SPALLATION NEUTRON SOURCE

This work was focused on understanding the neutrino fluxes but also explored the creation of other interesting particles. In particular, π^0, η^0, and π^- production are relevant to dark-matter searches using the SNS as an accelerator [61,62]. Here, we present some findings regarding the production of such particles using QGSP_BERT, noting that no effort was made in this work to specifically validate the production of any hadrons other than π^+. As mentioned in Sec. II, η production is excluded from our discussion here because it is not predicted by QGSP_BERT. Predictions with QGSP_BIC have previously been used with this simulation geometry to predict η flux for sensitivity studies [62].

Figure 15 shows the scattering angle as it relates to the creation energy for SNS-produced π^0 from 1 GeV incident protons on the top and 1.3 GeV incident protons on the bottom. We observe strong forward production for both, but note that we will have a small flux directed towards Neutrino Alley ($\cos\theta \approx 0$). This is relevant primarily for the π^0, which could decay in flight into dark-matter particles that cause an observable nuclear recoil in our CEvNS detectors. For π^-, dark matter could be produced in an absorption process or in a charge-exchange process; both are more efficient at nonrelativistic energies, and each would emit particles isotropically and negate any impact of forward production.

Assuming an aluminum PBW, the SNS produces 0.11 π^0/POT and 0.05 π^-/POT for 1 GeV incident protons. We also predict that the upgraded 1.3 GeV incident protons will produce 0.17 π^0/POT and 0.09 π^-/POT. This study also demonstrates the potential gain of the STS for dark-matter searches, particularly when equipped with forward-positioned detectors that reduce the distance to the target.

VII. ONGOING EFFORTS

In the absence of pion-production data for protons incident on Hg at energies up to 1.3 GeV, the ∼10% uncertainty assigned to our neutrino flux is a robust estimate that cannot be significantly improved through simulation. For the moment, the cross-section results on Ar

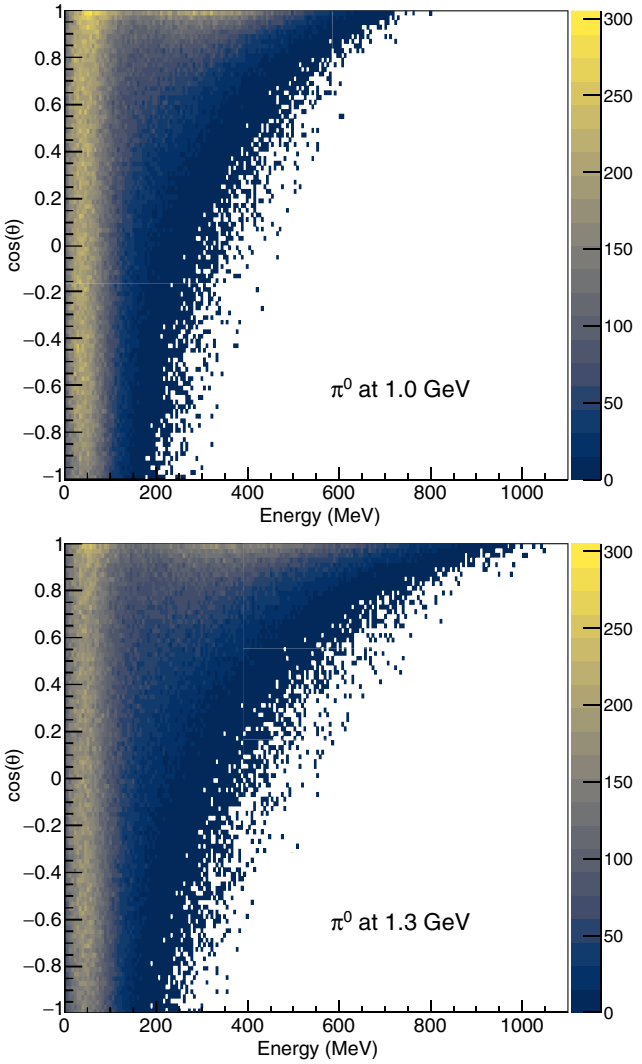

FIG. 15. Distribution of production angles and creation energies of π^0 at the SNS-FTS assuming an aluminum PBW. Top: using 1 GeV incident protons to mimic the current operating conditions of the SNS. Bottom: using 1.3 GeV incident protons to mimic the operating conditions following the upgrade.

are still dominated by statistical uncertainties [3], but the uncertainty on the neutrino flux is now the dominant uncertainty in the final results from CsI [20]. Two types of experimental measurements could further reduce this uncertainty.

Pion-production measurements with thin Hg targets would allow us to validate our simulation against interactions on the same material as the SNS target. The proposed EMPHATIC experiment at the Fermilab Test Beam Facility could measure differential pion-production cross sections on Hg at proton energies as low as 2 GeV with expected uncertainties less than 10% [63]. Meanwhile, the NA61/SHINE collaboration [64], which has measured pion production on both thin and replica targets for a variety of accelerator neutrino experiments, is investigating

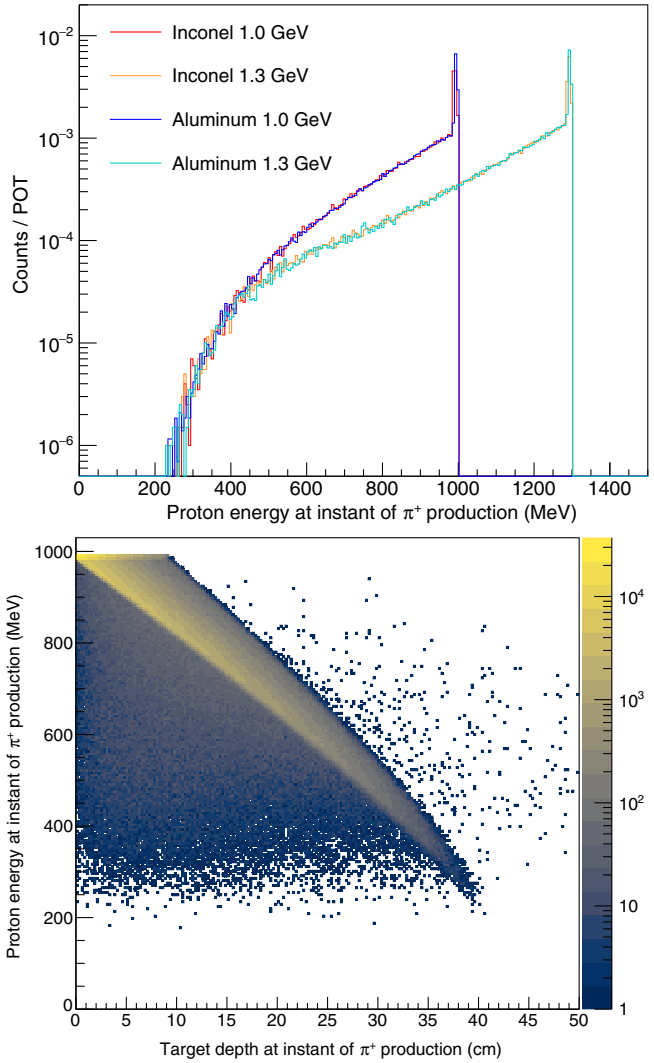

FIG. 16. Top: a histogram of the proton energies which produce π^+ at the SNS. Bottom: a closer look at how protons lose energy in the Hg target before creating π^+.

the possibility of reducing the energy of the CERN SPS H2 proton beamline to 1 GeV for low-energy pion-production studies [65]. These measurements will benefit neutrino experiments at the SNS and at other pion decay-at-rest neutrino sources with GeV-scale protons incident on a mercury target such as the JSNS^2 sterile-neutrino search at the Japan Spallation Neutron Source [66]. As a decay-at-rest source is insensitive to the production angle of the pion, new pion-production measurements should ideally cover as close to a 4π acceptance as possible.

Thin-target data at ≥ 1 GeV, however, cannot account for the effects of proton energy loss in the SNS target and from scattering in the PBW as shown in Fig. 16. Reducing our uncertainty using only thin-target data would require a dedicated measurement of the proton energy-loss profile within the SNS target that could be convolved with the observed pion production from thin-target data at varied energy. A separate approach to reducing neutrino-flux uncertainties would directly measure the total neutrino production at the SNS target. A D_2O detector, deployed at the SNS, would measure the charged-current interaction

$$\nu_e + d \rightarrow p + p + e^-. \tag{5}$$

The cross section of this reaction is well understood; theoretical calculations, taking several disparate approaches, have converged to the 2%–3% level [67,68]. A moderately sized detector, about 680 kg, could achieve similar statistical precision in about four SNS beam-years of operation. The observed ν_e flux from the SNS target could then be multiplied by three to obtain the total flux of all three neutrino flavors generated by π^+ decay. The COHERENT collaboration plans to build such a detector to directly normalize the simulated SNS neutrino flux [69]. We note that if the neutrino flux can be independently measured to high precision, one can in principle use neutrino data to validate models of hadron and neutrino production.

VIII. CONCLUSIONS

Using Geant4.10.06's standard QGSP_BERT physics list and treating the SNS as a point source, we predict a neutrino flux of $4.7 \times 10^7\ \nu\,\mathrm{cm}^{-2}\,\mathrm{s}^{-1}$ at 20 m from the target with ~99% of the total flux produced by the stopped π^+ decay chain for 1 GeV incident protons at the 1.4 MW First Target Station. Our calculation has a 10% uncertainty on the underlying pion-production model. This shared systematic for all COHERENT detectors is now the dominant uncertainty limiting precision CEvNS measurements, along with statistics in subsystems still taking data.

Our simulation remains an invaluable tool for estimating the flux of various particles at the SNS, the dependence of our predictions on the incident proton energy, and relative effects of the beamline geometry. In the future, we intend to use a modified version of this simulation to predict the low-energy contribution to the SNS neutrino flux from $\beta^\pm$ decays coincident with a proton spill resulting from activated materials. We also intend to use the framework we have developed here to perform model validation studies for particles such as π^0, π^- and η that are relevant for future dark-matter studies at the SNS.

ACKNOWLEDGMENTS

The COHERENT collaboration acknowledges the resources generously provided by the Spallation Neutron Source, a DOE Office of Science User Facility operated by the Oak Ridge National Laboratory. This work was supported by the US Department of Energy (DOE), Office of Science, Office of High Energy Physics and Office of Nuclear Physics; the National Science Foundation; the Consortium for Nonproliferation Enabling Capabilities; the

Korea National Research Foundation (NRF Grant No. 2022R1A3B1078756); the Ministry of Science and Higher Education of the Russian Federation (Project "Fundamental properties of elementary particles and cosmology" No. 0723-2020-0041); and the U.S. DOE Office of Science Graduate Student Research (SCGSR) program, administered for DOE by the Oak Ridge Institute for Science and Education which is in turn managed by Oak Ridge Associated Universities. The authors would also like to thank the Undergraduate Research Office of Carnegie Mellon University for their support on this project. Sandia National Laboratories is a multi-mission laboratory managed and operated by National Technology and Engineering Solutions of Sandia LLC, a wholly owned subsidiary of Honeywell International Inc., for the U.S. Department of Energy's National Nuclear Security Administration under Contract No. DE-NA0003525. The Triangle Universities Nuclear Laboratory is supported by the U.S. Department of Energy under Grant No. DE-FG02-97ER41033. Laboratory Directed Research and Development funds from Oak Ridge National Laboratory also supported this project. This research used the Oak Ridge Leadership Computing Facility, which is a DOE Office of Science User Facility.

[1] J. R. Haines, T. J. McManamy, T. A. Gabriel, R. E. Battle, K. K. Chipley, J. A. Crabtree, L. L. Jacobs, D. C. Lousteau, M. J. Rennich, and B. W. Riemer, Spallation neutron source target station design, development, and commissioning, Nucl. Instrum. Methods Phys. Res., Sect. A **764**, 94 (2014).

[2] D. Akimov *et al.* (COHERENT Collaboration), Observation of coherent elastic neutrino-nucleus scattering, Science **357**,1123 (2017).

[3] D. Akimov *et al.* (COHERENT Collaboration), First Measurement of Coherent Elastic Neutrino-Nucleus Scattering on Argon, Phys. Rev. Lett. **126**, 012002 (2021).

[4] D. Akimov *et al.* (COHERENT Collaboration), COHERENT 2018 at the Spallation Neutron Source, arXiv:1803.09183v2.

[5] J. Barranco, O. G. Miranda, and T. I. Rashba, Probing new physics with coherent neutrino scattering off nuclei, J. High Energy Phys. 12 (2005) 021.

[6] Patrick deNiverville, Maxim Pospelov, and Adam Ritz, Light new physics in coherent neutrino-nucleus scattering experiments, Phys. Rev. D **92**, 095005 (2015).

[7] P. Vogel and J. Engel, Neutrino electromagnetic form factors, Phys. Rev. D **39**, 3378 (1989).

[8] K. Scholberg, Prospects for measuring coherent neutrino nucleus elastic scattering at a stopped-pion neutrino source, Phys. Rev. D **73**, 033005 (2006).

[9] J. Papavassiliou, J. Bernabeu, and M. Passera, Neutrino-nuclear coherent scattering and the effective neutrino charge radius, Proc. Sci. HEP2005 (**2006**) 192, https://arxiv.org/abs/hep-ph/0512029.

[10] T. S. Kosmas, O. G. Miranda, D. K. Papoulias, M. Tórtola, and J. W. F. Valle, Probing neutrino magnetic moments at the Spallation Neutron Source facility, Phys. Rev. D **92**, 013011 (2015).

[11] M. Cadeddu, C. Giunti, K. A. Kouzakov, Y. F. Li, A. I. Studenikin, and Y. Y. Zhang, Neutrino charge radii from COHERENT elastic neutrino-nucleus scattering, Phys. Rev. D **98**, 113010 (2018).

[12] P. S. Amanik and G. C. McLaughlin, Nuclear neutron form factor from neutrino-nucleus coherent elastic scattering, J. Phys. G **36**, 015105 (2009).

[13] Kelly Patton, Jonathan Engel, Gail C. McLaughlin, and Nicolas Schunck, Neutrino-nucleus coherent scattering as a probe of neutron density distributions, Phys. Rev. C **86**, 024612 (2012).

[14] M. Cadeddu, C. Giunti, Y. F. Li, and Y. Y. Zhang, Average CsI Neutron Density Distribution from COHERENT Data, Phys. Rev. Lett. **120**, 072501 (2018).

[15] C. A. Duba *et al.*, HALO—the helium and lead observatory for supernova neutrinos, J. Phys. Conf. Ser. **136**, 042077 (2008).

[16] D. Väänänen and C. Volpe, The neutrino signal at HALO: Learning about the primary supernova neutrino fluxes and neutrino properties, J. Cosmol. Astropart. Phys. 10 (2011) 019.

[17] K. Langanke, P. Vogel, and E. Kolbe, Signal for Supernova ν_μ and ν_τ Neutrinos in Water Čerenkov Detectors, Phys. Rev. Lett. **76**, 2629 (1996).

[18] K. Scholberg, Supernova Neutrino Detection, Annu. Rev. Nucl. Part. Sci. **62**, 81 (2012).

[19] B. Abi *et al.* (DUNE Collaboration), Supernova neutrino burst detection with the deep underground neutrino experiment, Eur. Phys. J. C **81**, 423 (2021).

[20] D. Akimov *et al.* (COHERENT Collaboration), Measurement of the coherent elastic neutrino-nucleus scattering cross section on CsI by COHERENT, arXiv:2110.07730.

[21] S. Agostinelli *et al.* (GEANT4 Collaboration), GEANT4: A simulation toolkit, Nucl. Instrum. Methods Phys. Res., Sect. A **506**, 250 (2003).

[22] J. Allison *et al.*, Geant4 developments and applications, IEEE Trans. Nucl. Sci. **53**, 270 (2006).

[23] D. Akimov *et al.* (COHERENT Collaboration), A Geant4 simulation of particle production at the Spallation Neutron Source, 10.5281/zenodo.6391623 (2022).

[24] Hugo W. Bertini, Intranuclear-Cascade calculation of the secondary nucleon spectra from nucleon-nucleus interactions in the energy range 340 to 2900 MeV and comparisons with experiment, Phys. Rev. **188**, 1711 (1969).

[25] D. H. Wright and M. H. Kelsey, The Geant4 Bertini Cascade, Nucl. Instrum. Methods Phys. Res., Sect. A **804**, 175 (2015).

[26] G. Folger, V. N. Ivanchenko, and J. P. Wellisch, The binary cascade, Eur. Phys. J. A **21**, 407 (2004).

[27] A. Boudard, J. Cugnon, J.-C. David, S. Leray, and D. Mancusi, New potentialities of the Liège intranuclear cascade model for reactions induced by nucleons and light charged particles, Phys. Rev. C **87**, 014606 (2013).
[28] S. Leray, J. C. David, M. Khandaker, G. Mank, A. Mengoni, N. Otsuka, D. Filges, F. Gallmeier, A. Konobeyev, and R. Michel, Results from the IAEA benchmark of spallation models, J. Korean Phys. Soc. **59**, 791 (2011).
[29] S. Leray, D. Mancusi, P. Kaitaniemi, J. C. David, A. Boudard, B. Braunn, and J. Cugnon, Extension of the Liège Intra Nuclear Cascade model to light ion-induced collisions for medical and space applications, J. Phys. Conf. Ser. **420**, 012065 (2013).
[30] Richard E. Prael and Henry Lichtenstein, User guide to LCS: The LAHET code system, Report No. LA-UR-89-3014, 1989, https://mcnp.lanl.gov/pdf_files/la-ur-89-3014.pdf.
[31] R. L. Burman and P. Plischke, Neutrino fluxes from a high-intensity spallation neutron facility, Nucl. Instrum. Methods Phys. Res., Sect. A **398**, 147 (1997).
[32] R. L. Burman, A. C. Dodd, and P. Plischke, Neutrino flux calculations for the ISIS spallation neutron facility, Nucl. Instrum. Methods Phys. Res., Sect. A **368**, 416 (1996).
[33] R. L. Burman, M. E. Potter, and E. S. Smith, Monte Carlo simulation of neutrino production by medium-energy protons in a beam stop, Nucl. Instrum. Methods Phys. Res., Sect. A **291**, 621 (1990).
[34] D. R. F. Cochran, P. N. Dean, P. A. M. Gram, E. A. Knapp, E. R. Martin, D. E. Nagle, R. B. Perkins, W. J. Shlaer, H. A. Thiessen, and E. D. Theriot, Production of charged pions by 730-MeV protons from hydrogen and selected nuclei, Phys. Rev. D **6**, 3085 (1972).
[35] J. F. Crawford, M. Daum, G. H. Eaton, R. Frosch, H. Hirschmann, R. Horisberger, J. W. McCulloch, E. Steiner, R. Hausammann, R. Hess, and D. Werren, Measurement of cross sections and asymmetry parameters for the production of charged pions from various nuclei by 585-MeV protons, Phys. Rev. C **22**, 1184 (1980).
[36] John W. Norbury and Lawrence W. Townsend, Parameterized total cross sections for pion production in nuclear collisions, Nucl. Instrum. Methods Phys. Res., Sect. B **254**, 187 (2007).
[37] M. G. Catanesi *et al.* (HARP Collaboration), The HARP detector at the CERN PS, Nucl. Instrum. Methods Phys. Res., Sect. A **571**, 527 (2007).
[38] V. V. Abaev, E. P. Fedorova-Koval, A. B. Gridnev, V. P. Koptev, S. P. Kruglov, Yu. A. Malov, G. V. Shcherbakov, I. I. Stakovsky, and N. A. Tarasov, Inclusive pion production at the angles 0-degrees and 57.8-degrees in 1 GeV proton nucleus collisions, J. Phys. G **14**, 903 (1988).
[39] S. Nagamiya, M. -C. Lemaire, E. Moeller, S. Schnetzer, G. Shapiro, H. Steiner, and I. Tanihata, Production of pions and light fragments at large angles in high-energy nuclear collisions, Phys. Rev. C **24**, 971 (1981).
[40] A. Bolshakova *et al.* (HARP-CDP Collaboration), On the flaws in 'Official' HARP's data analysis, https://cds.cern.ch/record/1137133/files/SPSC-SR-037.pdf (2008).
[41] M. G. Catanesi *et al.* (HARP Collaboration), Large-angle production of charged pions by 3-GeV/c–12.9-GeV/c protons on beryllium, aluminium and lead targets, Eur. Phys. J. C **54**, 37 (2008).
[42] M. G. Catanesi *et al.* (HARP Collaboration), Large-angle production of charged pions by 3-GeV/c–12-GeV/c protons on carbon, copper and tin targets, Eur. Phys. J. C **53**, 177 (2008).
[43] A. Bolshakova *et al.* (HARP-CDP Collaboration), Cross-sections of large-angle hadron production in proton- and pion-nucleus interactions VI: Carbon nuclei and beam momenta from ±3 GeV/c to ±15 GeV/c, Eur. Phys. J. C **70**, 573 (2010).
[44] A. Bolshakova *et al.* (HARP-CDP Collaboration), Cross-sections of large-angle hadron production in proton–and pion–nucleus interactions VIII: Aluminium nuclei and beam momenta from ±3 GeV/c to ±15 GeV/c, Eur. Phys. J. C **72**, 1882 (2012).
[45] A. Bolshakova *et al.* (HARP-CDP Collaboration), Cross-sections of large-angle hadron production in proton- and pion-nucleus interactions VII: Tin nuclei and beam momenta from ±3 GeV/c to ±5 GeV/c, Eur. Phys. J. C **71**, 1719 (2011).
[46] M. G. Catanesi *et al.* (HARP Collaboration), Large-angle production of charged pions with 3-12.9-GeV/c incident protons on nuclear targets, Phys. Rev. C **77**, 055207 (2008).
[47] A. Bolshakova *et al.* (HARP-CDP Collaboration), Cross-sections of large-angle hadron production in proton- and pion-nucleus interactions. III. Tantalum nuclei and beam momenta from ±3 GeV/c to ±15 GeV/c, Eur. Phys. J. C **63**, 549 (2009).
[48] A. Bolshakova *et al.* (HARP-CDP Collaboration), Cross-sections of large-angle hadron production in proton- and pion-nucleus interactions V: Lead nuclei and beam momenta from ±3 GeV/c to ±15 GeV/c, Eur. Phys. J. C **66**, 57 (2010).
[49] J. Apostolakis *et al.*, Progress in Geant4 electromagnetic physics modelling and validation, J. Phys. Conf. Ser. **664**, 072021 (2015).
[50] J. Allison *et al.*, Recent developments in Geant4, Nucl. Instrum. Methods Phys. Res., Sect. A **835**, 186 (2016).
[51] L. Aliaga *et al.* (MINERνA Collaboration), Neutrino flux predictions for the NuMI beam, Phys. Rev. D **94**, 092005 (2016).
[52] Ethan Tuttle, Updating hadron production models to better predict neutrino flux for DUNE, 10.2172/1661678 (2020).
[53] ORNL, Spallation Neutron Source manufacturing study drawings (private communication).
[54] Special Metals, INCONEL Alloy 718, https://www.specialmetals.com/documents/technical-bulletins/inconel/inconel-alloy-718.pdf (2021).
[55] S. Henderson *et al.*, The Spallation Neutron Source accelerator system design, Nucl. Instrum. Methods Phys. Res., Sect. A **763**, 610 (2014).
[56] Willem Blokland, T. McManamy, and T. Shea, SNS target imaging system software and analysis, in *Proceedings of the BIW10, Santa Fe, New Mexico (2010)* (JACoW, 2010), https://accelconf.web.cern.ch/BIW2010/papers/tupsm003.pdf.
[57] J. Galambos *et al.*, Conceptual design report: Proton power upgrade project, Report No. ORNL/TM-2016/672, 2017, https://neutrons.ornl.gov/sites/default/files/PPU%20CDR_withAuthors.pdf.
[58] J. Galambos and D. Anderson *et al.*, Technical design report: Second target station, Report No. ORNL/TM-2015/24,

2015, https://neutrons.ornl.gov/sites/default/files/SNS_STS_Technical_Design_Report_2015-01.pdf.

[59] Proceedings of the Workshop on Fundamental Physics at the Second Target Station (FPSTS19), (2019), https://conference.sns.gov/event/171/.

[60] J. Asaadi *et al.*, Neutrino opportunities at the ORNL second target station, (2020), Snowmass letter of interest, https://www.snowmass21.org/docs/files/summaries/NF/SNOWMASS21-NF6_NF9-CF1_CF0-TF11_TF0-IF2_IF8_Kate_Scholberg-161.pdf.

[61] Bhaskar Dutta, Doojin Kim, Shu Liao, Jong-Chul Park, Seodong Shin, and Louis E. Strigari, Dark Matter Signals from Timing Spectra at Neutrino Experiments, Phys. Rev. Lett. **124**, 121802 (2020).

[62] D. Akimov *et al.* (COHERENT Collaboration), Sensitivity of the COHERENT experiment to accelerator-produced dark matter, Phys. Rev. D **102**, 052007 (2020).

[63] T. Akaishi *et al.*, EMPHATIC: A proposed experiment to measure hadron scattering and production cross sections for improved neutrino flux predictions, arXiv:1912.08841.

[64] N. Abgrall *et al.* (NA61/SHINE Collaboration), NA61/SHINE facility at the CERN SPS: Beams and detector system, J. Instrum. **9**, P06005 (2014).

[65] NA61/SHINE at Low Energy Workshop (2020), https://indico.cern.ch/event/973899/contributions/.

[66] S. Ajimura *et al.* (JSNS^2 Collaboration), Technical design report: Searching for a sterile neutrino at J-PARC MLF, arXiv:1705.08629.

[67] B. Mosconi, P. Ricci, E. Truhlík, and P. Vogel, Model dependence of the neutrino-deuteron disintegration cross sections at low energies, Phys. Rev. C **75**, 044610 (2007).

[68] Shung-Ichi Ando, Young-Ho Song, and Chang Ho Hyun, Neutrino-deuteron reactions at solar neutrino energies in pionless effective field theory with dibaryon fields, Phys. Rev. C **101**, 054001 (2020).

[69] D. Akimov *et al.* (COHERENT Collaboration), A D_2O detector for flux normalization of a pion decay-at-rest neutrino source, J. Instrum. **16**, P08048 (2021).